

Full-Bridge Three-Port Converters With Wide Input Voltage Range for Renewable Power Systems

Hongfei Wu, *Student Member, IEEE*, Kai Sun, *Member, IEEE*, Runruo Chen, Haibing Hu, *Member, IEEE*, and Yan Xing, *Member, IEEE*

Abstract—A systematic method for deriving three-port converters (TPCs) from the full-bridge converter (FBC) is proposed in this paper. The proposed method splits the two switching legs of the FBC into two switching cells with different sources and allows a dc bias current in the transformer. By using this systematic method, a novel full-bridge TPC (FB-TPC) is developed for renewable power system applications which features simple topologies and control, a reduced number of devices, and single-stage power conversion between any two of the three ports. The proposed FB-TPC consists of two bidirectional ports and an isolated output port. The primary circuit of the converter functions as a buck-boost converter and provides a power flow path between the ports on the primary side. The FB-TPC can adapt to a wide source voltage range, and tight control over two of the three ports can be achieved while the third port provides the power balance in the system. Furthermore, the energy stored in the leakage inductance of the transformer is utilized to achieve zero-voltage switching for all the primary-side switches. The FB-TPC is analyzed in detail with operational principles, design considerations, and a pulsewidth modulation scheme (PWM), which aims to decrease the dc bias of the transformer. Experimental results verify the feasibility and effectiveness of the developed FB-TPC. The topology generation concept is further extended, and some novel TPCs, dual-input, and multiport converters are presented.

Index Terms—Boost-buck, dc-dc converter, full-bridge converter (FBC), renewable power system, three-port converter (TPC).

I. INTRODUCTION

RENEWABLE power systems, which are capable of harvesting energy from, for example, solar cells, fuel cells, wind, and thermoelectric generators, are found in many applications such as hybrid electric vehicles, satellites, traffic lights, and powering remote communication systems. Since the output

power of renewable sources is stochastic and the sources lack energy storage capabilities, energy storage systems such as a battery or a supercapacitor are required to improve the system dynamics and steady-state characteristics. A three-port converter (TPC), which can interface with renewable sources, storage elements, and loads, simultaneously, is a good candidate for a renewable power system and has recently attracted increased research interest [1]–[18].

Compared with the conventional solutions that employ multiple converters, the TPC features single-stage conversion between any two of the three ports, higher system efficiency, fewer components, faster response, compact packaging, and unified power management among the ports with centralized control [1]–[5]. As a result of these remarkable merits, many TPCs have been proposed recently for a variety of applications. One way to construct a TPC is to interface several conversion stages to a common dc bus [3]–[5]. But this is not an integrated solution since only a few devices are shared. Some TPCs are constructed from full-bridge, half-bridge, or series-resonant topologies by utilizing the magnetic coupling through a multiwinding transformer [9]–[15]. Power flow control and zero-voltage switching (ZVS) are achieved with phase-shift control between different switching bridges, whose principles are the same as the dual-active-bridge (DAB) topology [16], [17]. Isolation and bidirectional capabilities can also be achieved with these topologies. However, too many active switches have been used, resulting in a complicated driving and control circuit, which may degrade the reliability and performance of the integrated converters. In [18], a boost-integrated TPC is proposed based on the phase-shift full-bridge converter (FBC) and power flow control is implemented with pulsewidth modulation (PWM) plus phase-shift control. This principle is further extended to the three-phase FBC in [19]. A trimodal half-bridge converter is developed from a half-bridge converter in [6]–[8] to implement three-port interface. This converter can be regarded as a buck-integrated TPC because the primary circuit of the half-bridge converter functions as a buck converter to bridge the power flow path between the input source and the battery. These TPCs offer low component counts and simple control. However, because the equivalent conversion circuit between the input source and energy storage element is a step-up or step-down converter with limited voltage conversion ratio, they are not flexible enough for applications where the voltage of the source port, such as solar, fuel cells, and thermoelectric generator, varies over a wide range.

The major contribution of this paper is to propose a systematic method for generating TPC topologies from FBCs and to

Manuscript received September 7, 2011; revised December 21, 2011; accepted February 8, 2012. Date of current version May 15, 2012. This work was supported by the National Natural Science Foundation of China (Project 51077071), by the project of outstanding discipline construction, Jiangsu, China, Tsinghua University Initiative Scientific Research Program (20101081909), and by the State Key Laboratory of Power Systems, Tsinghua University under Grant SKLD10KM02 and Grant SKLD10M09. Recommended for publication by Associate Editor P. C. Loh.

H. Wu, R. Chen, H. Hu, and Y. Xing are with the Jiangsu Key Laboratory of New Energy Generation and Power Conversion, College of Automation Engineering, Nanjing University of Aeronautics and Astronautics, Nanjing 210016, China (e-mail: wuhongfei@nuaa.edu.cn; chenrunruo@nuaa.edu.cn; huhaibing@nuaa.edu.cn; xingyan@nuaa.edu.cn).

K. Sun is with the State Key Laboratory of Power Systems, Department of Electrical Engineering, Tsinghua University, Beijing 100084, China (e-mail: sun-kai@mail.tsinghua.edu.cn).

Color versions of one or more of the figures in this paper are available online at <http://ieeexplore.ieee.org>.

Digital Object Identifier 10.1109/TPEL.2012.2188105

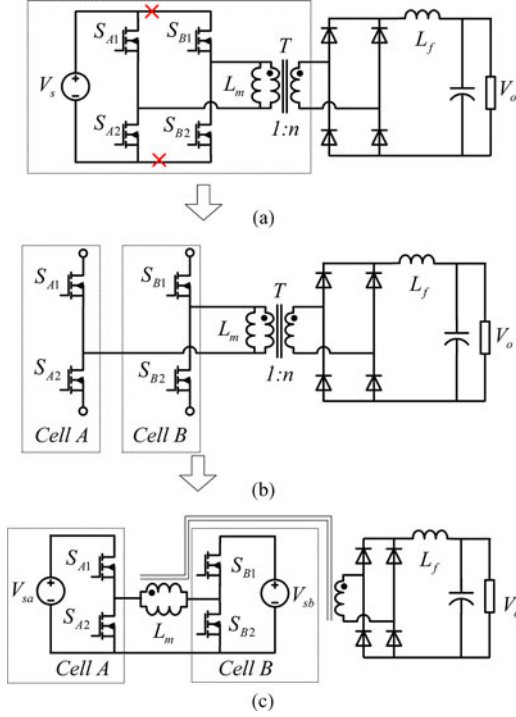


Fig. 1. Proposed derivation of full-bridge three-port converter. (a) Full-bridge converter. (b) Two-switching cells. (c) Full-bridge three-port converter.

find a novel full-bridge TPC (FB-TPC) with single-stage power conversion between any two of the three ports. Furthermore, from a topological point of view, because a buck-boost converter is integrated in the proposed FB-TPC, it can adapt to applications with a wide source voltage range. ZVS of all the primary-side switches can also be achieved with the proposed FB-TPC. This paper is organized as follows. In Section II, the basic ideas used to generate FB-TPC are proposed. In Section III, the FB-TPC is analyzed in detail, with operation principles, design considerations, and modulation methods given to verify the proposed method. Experimental results are presented in Section IV. The topology generation method of the FB-TPC is further extended in Section V. Finally, conclusions will be given in Section VI.

II. DERIVATION OF THE FB-TPC FROM A FULL-BRIDGE DC-DC CONVERTER

Referring to Fig. 1(a), the primary side of the FBC consists of two switching legs, composed of S_{A1} , S_{A2} and S_{B1} , S_{B2} , in parallel, connected to a common input source V_s . For the primary side of the FBC, the constraint condition of the operation of the FBC is the voltage-second balance principle of the magnetizing inductor L_m . This means that, from a topological point of view, the two switching legs of the FBC can also be split into two symmetrical parts, cells A and B, if only L_m satisfies the voltage-second balance principle, as shown in Fig. 1(b). The two cells can be connected to different sources, V_{sa} and V_{sb} , respectively, as shown in Fig. 1(c), and then a novel FB-TPC is derived. The voltage of the two sources of the FB-TPC can be

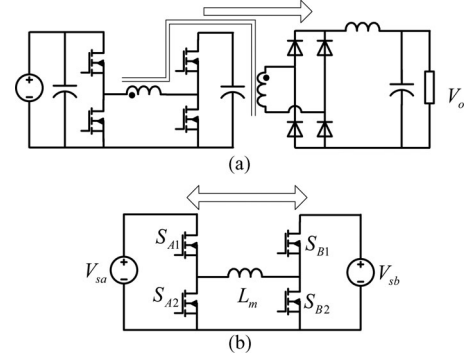


Fig. 2. Equivalent circuits. (a) Between source and load. (b) Between the two sources.

arbitrary. Specially, if V_{sa} always equals V_{sb} , the two cells can be paralleled directly and then the conventional FBC is derived. Therefore, the FBC can be seen as a special case of the FB-TPC as shown in Fig. 1(c).

Close observation indicates that the FB-TPC has a symmetrical structure and both V_{sa} and V_{sb} can supply power to the load V_o . The equivalent circuit from one of the source ports to the load port is shown in Fig. 2(a). In addition, a bidirectional buck-boost converter [20]–[22] is also integrated in the primary side of the FB-TPC by employing the magnetizing inductor of the transformer L_m as a filter inductor. With the bidirectional buck-boost converter, the power flow paths between the two sources, V_{sa} and V_{sb} , can be configured and the power can be transferred between V_{sa} and V_{sb} freely. The equivalent circuit between the two sources is illustrated in Fig. 2(b). According to the equivalent circuits shown in Fig. 2, it can be seen that the power flow paths between any two of the three ports, V_{sa} , V_{sb} , and V_o , have been built. The unique characteristics of the FB-TPC are analyzed and summarized as follows.

- 1) The FB-TPC has two bidirectional ports and one isolated output port. Single-stage power conversion between any two of the three ports is achieved. The FB-TPC is suitable for renewable power systems and can be connected with an input source and an energy storage element, such as the photovoltaic (PV) with a battery backup, or with two energy storage elements, such as the hybrid battery and the supercapacitor power system.
- 2) A buck-boost converter is integrated in the primary side of the FB-TPC. With the integrated converter, the source voltage V_{sa} can be either higher or lower than V_{sb} , and vice versa. This indicates that the converter allows the sources' voltage varies over a wide range.
- 3) The devices of the FB-TPC are the same as the FBC and no additional devices are introduced which means high integration is achieved.
- 4) The following analysis will indicate that all four active switches in the primary side of the FB-TPC can be operated with ZVS by utilizing the energy stored in the leakage inductor of the transformer, whose principle is similar to the phase-shift FBC.

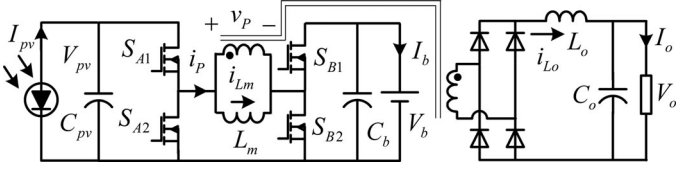


Fig. 3. Topology of the proposed FB-TPC.

TABLE I
OPERATION MODES OF THE FB-TPC

Operation modes	Power of PV	Power of battery
Dual-output mode	$p_{pv} \geq p_o$	Battery charging, $p_b \geq 0$
Dual-input mode	$p_{pv} \leq p_o, p_{pv} > 0$	Battery discharging, $p_b < 0$
Single-input single-output mode	$p_{pv} = 0$	Battery discharging, $p_b = -p_o$

III. ANALYSIS OF THE FB-TPC FOR THE STAND-ALONE RENEWABLE POWER SYSTEM APPLICATION

The FB-TPC, as shown in Fig. 1(b), is applied to a stand-alone PV power system with battery backup to verify the proposed topology. To better analyze the operation principle, the proposed FB-TPC topology is redrawn in Fig. 3, the two source ports are connected to a PV source and a battery, respectively, while the output port is connected to a load.

There are three power flows in the standalone PV power system: 1) from PV to load; 2) from PV to battery; and 3) from battery to load. As for the FB-TPC, the load port usually has to be tightly regulated to meet the load requirements, while the input port from the PV source should implement the maximum power tracking to harvest the most energy. Therefore, the mismatch in power between the PV source and load has to be charged into or discharged from the battery port, which means that in the FB-TPC, two of the three ports should be controlled independently and the third one used for power balance. As a result, two independently controlled variables are necessary.

A. Switching State Analysis

Ignoring the power loss in the conversion, we have

$$p_{pv} = p_b + p_o \quad (1)$$

where p_{pv} , p_b , and p_o are the power flows through the PV, battery, and load port, respectively. The FB-TPC has three possible operation modes: 1) dual-output (DO) mode, with $p_{pv} \geq p_o$, the battery absorbs the surplus solar power and both the load and battery take the power from PV; (2) dual-input (DI) mode, with $p_{pv} \leq p_o$ and $p_{pv} > 0$, the battery discharges to feed the load along with the PV; and (3) single-input single-output (SISO) mode, with $p_{pv} = 0$, the battery supplies the load power alone. When $p_{pv} = p_o$ exactly, the solar supplies the load power alone and the converter operates in a boundary state of DI and DO modes. This state can either be treated as DI or DO mode. Since the FB-TPC has a symmetrical structure, the operation of the converter in this state is the same as that of SISO mode, where the battery feeds the load alone. The operation modes and power flows of the converter are listed in Table I. The power flow paths/directions of each operation mode have been illustrated in Fig. 4.

The switching states in different operation modes are the same and the difference between these modes are the value and direction of i_{Lm} , as shown in Fig. 3, which is dependent on the power of p_{pv} and p_o . In the DO mode, i_{Lm} is positive, in the SISO mode, i_{Lm} is negative, and in the DI mode, i_{Lm} can either

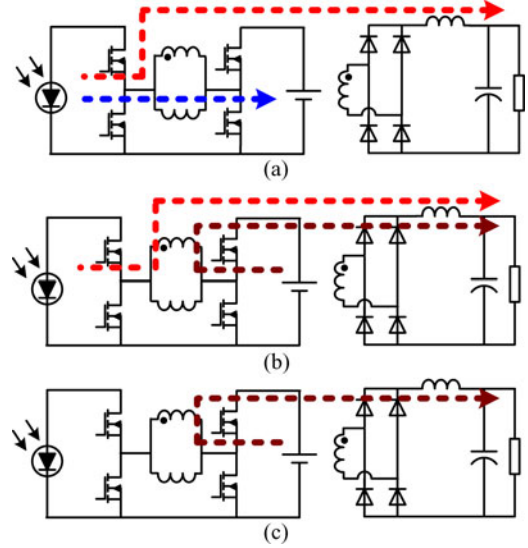


Fig. 4. Power flow paths/directions of each operation mode. (a) DO mode. (b) DI mode. (c) SISO mode.

be positive or negative. Take the DO mode as an example to analyze.

For simplicity, the following assumptions are made: 1) C_{pv} , C_b , and C_o are large enough and the voltages of the three ports, V_{pv} , V_b , and V_o , are constant during the steady state; and 2) the $V_{pv} \geq V_b$ case is taken as an example for the switching state analysis.

There are four switching states in one switching cycle. The key waveforms and the equivalent circuit in each state are shown in Figs. 5 and 6, respectively.

State I [t_0-t_1]: Before t_0 , S_{A2} and S_{B2} are ON and S_{A1} and S_{B1} are OFF, while i_{Lm} freewheels through S_{A2} and S_{B2} . At t_0 , S_{A1} turns ON and S_{A2} turns OFF. A positive voltage is applied across the transformer's primary winding [see Fig. 6(a)]

$$\begin{cases} \frac{di_{Lm}}{dt} = \frac{V_{pv}}{L_m} \\ \frac{di_{Lo}}{dt} = \frac{nV_{pv} - V_o}{L_o} \\ i_P = i_{Lm} + ni_{Lo}. \end{cases} \quad (2)$$

State II [t_1-t_2]: At t_1 , S_{B2} turns OFF and S_{B1} turns ON. A positive voltage is applied on the primary winding of the

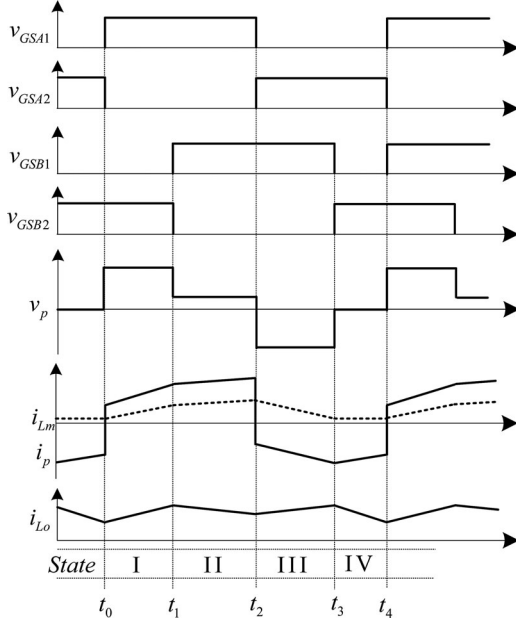
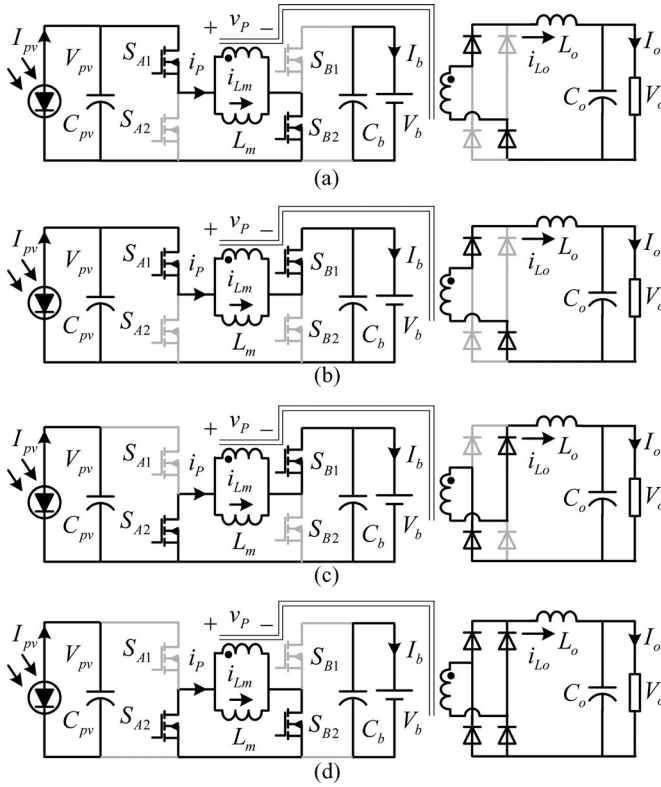


Fig. 5. Key waveforms of the FB-TPC.

Fig. 6. Equivalent circuits of each switching state. (a) $[t_0, t_1]$. (b) $[t_1, t_2]$. (c) $[t_2, t_3]$. (d) $[t_3, t_4]$.

transformer [see Fig. 6(b)]

$$\begin{cases} \frac{di_{Lm}}{dt} = \frac{V_{pv} - V_b}{L_m} \\ \frac{di_{Lo}}{dt} = \frac{n(V_{pv} - V_b) - V_o}{L_o} \\ i_p = i_{Lm} + ni_{Lo} \end{cases} \quad (3)$$

State III $[t_2-t_3]$: At t_2 , S_{A1} turns OFF and S_{A2} turns ON. A negative voltage is applied on the primary winding of the transformer [see Fig. 6(c)]

$$\begin{cases} \frac{di_{Lm}}{dt} = -\frac{V_b}{L_m} \\ \frac{di_{Lo}}{dt} = \frac{nV_b - V_o}{L_o} \\ i_p = i_{Lm} - ni_{Lo} \end{cases} \quad (4)$$

State IV $[t_3-t_4]$: At t_3 , S_{B1} turns OFF and S_{B2} turns ON. The voltage across the primary winding is clamped at zero, and i_{Lm} freewheels through S_{A2} and S_{B2} [see Fig. 6(d)]

$$\begin{cases} \frac{di_{Lm}}{dt} = 0 \\ \frac{di_{Lo}}{dt} = -\frac{V_o}{L_o} \end{cases} \quad (5)$$

Applying the volt-second balance principle to the magnetizing inductor of the transformer L_m and the output filter inductor L_o , respectively, we obtain that the following:

$$V_{pv} = \frac{D_{B1}}{D_{A1}} V_b \quad (6)$$

$$V_o = n[D_1 V_{pv} + D_2 (V_{pv} - V_b) + D_3 V_b] = 2nD_3 V_b \quad (7)$$

where D_{A1} and D_{B1} are the duty cycles of S_{A1} and S_{B1} in the steady state, respectively, and D_1 – D_3 are the equivalent duty cycles of States I–III, especially, D_3 is the overlapped section of the driven signal for S_{A1} and S_{B2} .

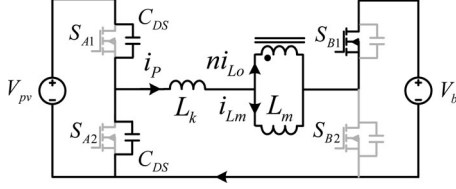
For the $V_{pv} < V_b$ case, the operation principles of the FB-TPC are the same as those of the $V_{pv} \geq V_b$ case. The differences between these two cases are the voltage applied to the transformer and the direction of the reflected current of i_{Lo} through primary windings. By following the same analysis procedure, the output voltage V_o can be given by

$$V_o = n[D_1 V_{pv} + D_2 (V_b - V_{pv}) + D_3 V_b] = 2nD_1 V_{pv} \quad (8)$$

It can be seen from (6)–(8) that the voltage of the PV source V_{pv} can be regulated with D_{A1} and D_{B1} for the maximum power point tracking (MPPT), taking the battery voltage V_b as constant. The output voltage V_o can be tightly regulated with D_1 and D_3 . This means that there are two independent control variables to achieve the power flow control over two of the three ports of the HB-TPC.

B. ZVS Analysis

According to the analysis, the operation of the FB-TPC is similar to the operation of a phase-shift FBC [23], [24] with the two switches S_{A1} (S_{B1}) and S_{A2} (S_{B2}), driven with complementary signals. The proposed FB-TPC can utilize the leakage inductance, filter inductance, and the output capacitors (parasitic drain to source capacitors) of the switches to realize ZVS, zero-voltage turn-ON, and zero-voltage turn-OFF for all the switches. The operation principle is similar to the phase-shift FBC [23], [24]. The only difference is that in the proposed FB-TPC, the magnetizing inductor of the transformer L_m can also help to achieve ZVS of the switches if the direction of i_{Lm} is the

Fig. 7. ZVS analysis of S_{A2} .

same as i_P . Take S_{A2} as an example. As shown in Fig. 7, where only the primary circuit is shown for simplicity, considering the leakage inductance L_k , when S_{B1} is ON and S_{A1} is turned OFF, $i_P = i_{Lm} + ni_{Lo}$, the energy stored in L_k and L_m will release to charge or discharge the parasitic drain to source capacitors of S_{A1} and S_{A2} . As a result, with a proper dead time, ZVS of S_{A2} can be achieved if the following condition is satisfied

$$\frac{1}{2} [L_k(i_{Lm} + ni_{Lo})^2 + L_m i_{Lm}^2] > C_{DS} V_b^2. \quad (9)$$

C. Design Consideration

As for the semiconductor device stress, the FB-TPC is similar to the traditional FBC. But a key difference between these two converters is that the magnetizing inductance of the transformer L_m is operated as an inductor as well. We also take the $V_{pv} \geq V_b$ case as an example for analysis.

From (1), in the steady state, we have

$$V_{pv} I_{pv} = V_b I_b + V_o I_o. \quad (10)$$

According to the switching states I and II, we have

$$I_{pv} = D_{A1}(I_{Lm} + nI_o) \quad (11)$$

where I_{Lm} is the average magnetizing current of the transformer, and then we have

$$I_{Lm} = \frac{I_{pv}}{D_{A1}} - nI_o. \quad (12)$$

From (12), it can be seen that the larger the D_{A1} , the smaller the I_{Lm} .

According to the switching states II and III, we have

$$\begin{aligned} I_b &= D_2(I_{Lm} + nI_o) - D_3(I_{Lm} - nI_o) \\ &= (D_{B1} - 2D_3)I_{Lm} + D_{B1}nI_o. \end{aligned} \quad (13)$$

Then the average transformer magnetizing current I_{Lm} can also be given by the following equation:

$$I_{Lm} = \frac{I_b - D_{B1}nI_o}{D_{B1} - 2D_3}. \quad (14)$$

According to (7), D_3 is determined by V_b and V_o , therefore, the larger the D_{B1} the smaller the I_{Lm} .

It is noticed that I_{Lm} can be reduced by increasing the nominal values of D_{A1} and D_{B1} ; this result is also valid for the $V_{pv} < V_b$ case by following the same analysis procedure. Therefore, the value of I_{Lm} can be decreased with a properly designed modulation scheme.

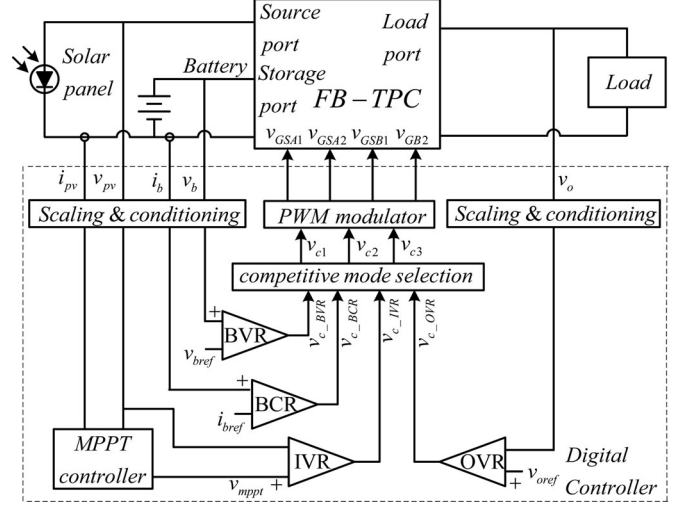


Fig. 8. Control diagram for the three-port converter [6].

D. Pulsewidth Modulation

The power management and the control for the TPC proposed in [6] are applied to the FB-TPC because the power control of the renewable power system with battery backup follows a similar principle and has nothing to do with the type of topology. However, the PWM schemes of different converters are usually different from each other and mainly determined by the topology. For better analysis of the PWM scheme of the FB-TPC, the control diagram for the power system is redrawn in Fig. 8 [6]. Four regulators, PV voltage regulator (IVR) for MPPT, battery voltage regulator (BVR) for maximum voltage charging control, battery current regulator (BCR) for maximum current charging control, and output voltage regulator (OVR) for output voltage control, are used to implement the power management of the system. With the control diagram shown in Fig. 8, the FB-TPC can work in the DO, DI, or SISO mode, depending on the relationship between the PV power and load power. The operating principle is similar to that described in [6].

Different PWM schemes can be applied to the proposed FB-TPC. However, according to (12) and (14), I_{Lm} can be decreased by increasing D_{A1} and D_{B1} . To decrease the magnetizing inductor's current of the transformer, D_{A1} and D_{B1} should be as large as possible.

According to the switching state analysis, it can be seen that, as shown in Fig. 5, the smaller the D_1 , the larger the D_{B1} ; therefore, the maximum value of D_{B1} is

$$D_{B1_max} = D_{A1} + D_3 \quad (15)$$

and the maximum value of D_{A1} is determined by D_3

$$D_{A1_max} = 1 - D_3. \quad (16)$$

Based on the analysis, the proposed PWM scheme and its generation are illustrated in Fig. 9, where V_{tri} is the peak-to-peak value of the carrier voltage v_{tri} , and v_{c1} , v_{c2} , v_{c3} are control voltages generated by using a competitive method and given by

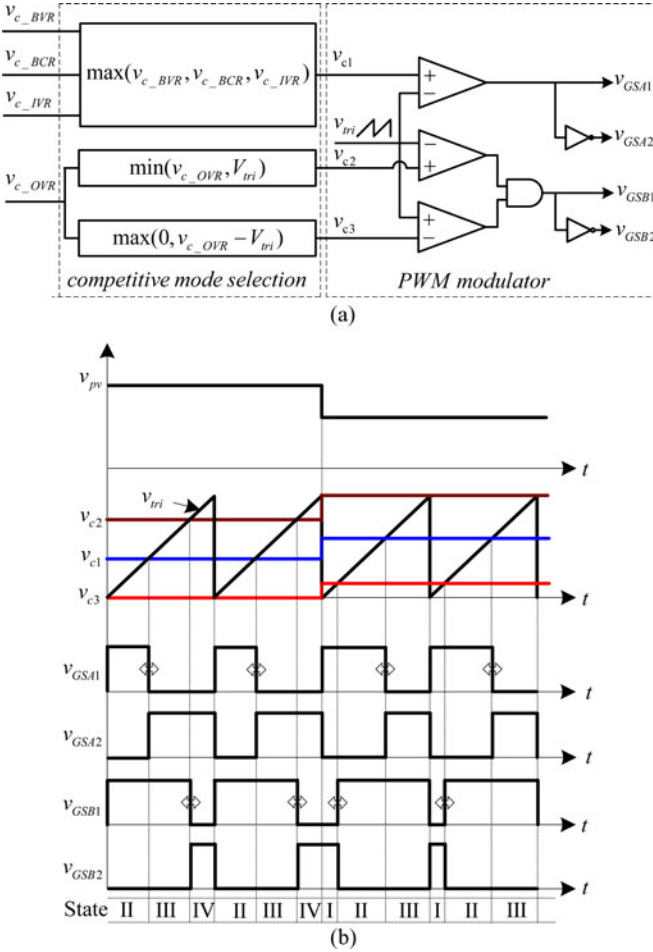


Fig. 9. PWM scheme for the FB-TPC. (a) PWM generation. (b) Key waveforms.

the following equations:

$$\begin{cases} v_{c1} = \max(v_{c_BVR}, v_{c_BCR}, v_{c_IVR}) \\ v_{c2} = \min(v_{c2}, V_{tri}) \\ v_{c3} = \max(0, v_{c2} - V_{tri}). \end{cases} \quad (17)$$

With the proposed PWM scheme, when v_{pv} is much higher than v_b , $v_{c2} < V_{tri}$, and v_{c3} stays at zero, D_{B1} will reach its maximum value, given by (15), as shown in Fig. 9(b). There are only three switching states, states II–IV, in one switching cycle. This means that by regulating the turned OFF time of S_{A1} with v_{c1} , the PV power can be controlled to achieve the MPPT, or battery charging control and output voltage v_o is further controlled with v_{c2} regulating D_3 by adjusting the turned OFF time of S_{B1} . When v_{pv} decreases and $v_{c2} \leq V_{tri}$, D_{A1} will reach its maximum value, given by (16), $v_{c2} = V_{tri}$ and $v_{c3} \geq 0$, then v_o is controlled with v_{c2} by regulating the turned ON time of S_{B1} , as shown in Fig. 9(b), and there are three switching states, states I–III, in one switching cycle.

With the proposed PWM scheme, the converter can adapt to different input voltages while minimizing the magnetizing inductor's current of the transformer.

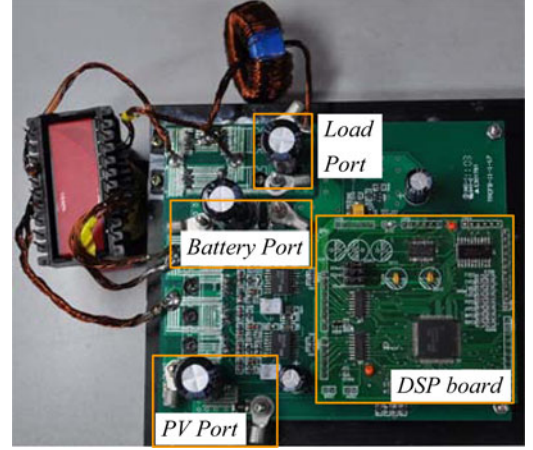


Fig. 10. Picture of the prototype.

TABLE II
CIRCUIT PARAMETERS

v_{pv}	38V~76V	p_{in}	0~300W
v_o	42V	p_o	0~180W
v_b	26V~38V	C_{pv}, C_b, C_o	470uF
L_m	70uH	L_o	100uH
Turns ratio (n)	3:4	$S_{A1}, S_{A2}, S_{B1}, S_{B2}$	IRF3710
Rectifier diodes	SRF20200C	Switching frequency	100kHz

IV. EXPERIMENTAL RESULTS

An FB-TPC prototype controlled by a TMS320F2808 DSP, as shown in Fig. 10, is built with the key parameters listed in Table II. A variable resistor in series with a dc source is used to simulate the PV characteristics.

The steady-state waveforms of the converter with 55 V input voltage at full load are shown in Fig. 11. Fig. 11(a) shows the waveforms under the DO mode and Fig. 11(b) shows the waveforms of the DI mode. It can be seen that the shapes of the corresponding waveforms are the same and the only difference is the average value of the primary winding's current i_p . In Fig. 11(a), the average value of i_p is positive while in Fig. 11(b) i_p is negative. With this input voltage, $v_{c2} \leq V_{tri}$ and D_{A1} reaches its maximum value, the converter switches among states I–III alternately in one switching cycle, as shown in the right part of Fig. 9(b). The steady-state waveforms of the converter in DO mode with 70 V input voltage at full load are given in Fig. 12. With this input voltage, $v_{c2} > V_{tri}$ and D_{B1} reaches its maximum value. The converter switches among states II–IV alternately in one switching cycle, as shown in the left part of Fig. 9(b).

The driving voltage and drain to source voltage on S_{A1} , S_{A2} , S_{B1} , and S_{B2} , in the DO mode at full load, is given in Fig. 13, which indicates that all the switches are turned ON with ZVS and the voltage spike on switches is very small when switches are turned OFF.

Fig. 14 shows the transient waveforms with stepping up (from half load to full load) and stepping down (from full load to half load) the load resistors. It can be seen that when the output load transitions between half load and full load, the converter

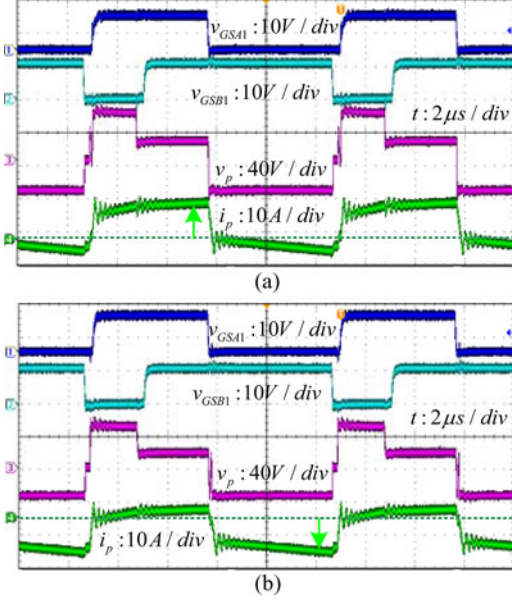


Fig. 11. Steady-state waveforms at 55 V input voltage with full-load condition in (a) dual-output mode and (b) dual-input mode.

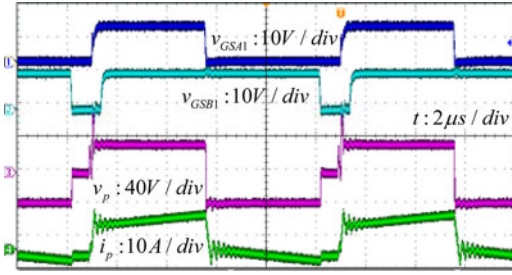


Fig. 12. Steady-state waveforms at 70 V input voltage with full-load condition in dual-output mode.

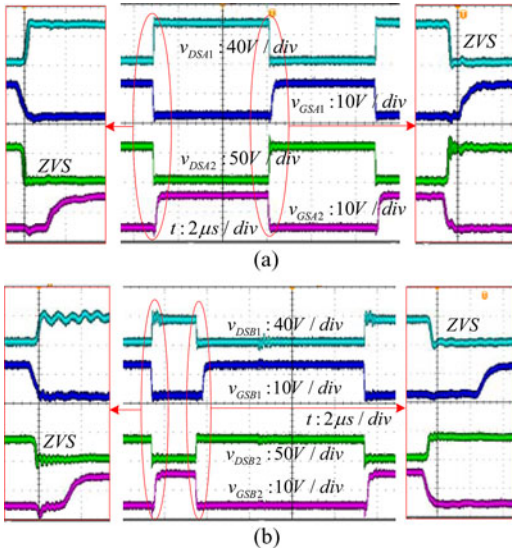


Fig. 13. Driving voltage and drain to source voltage of (a) S_{A1} and S_{A2} and (b) S_{B1} and S_{B2} .

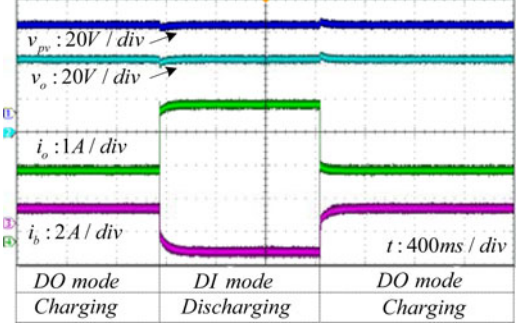


Fig. 14. Load transient waveforms by stepping up (half load to full load) and stepping down (full load to half load) load resistors.

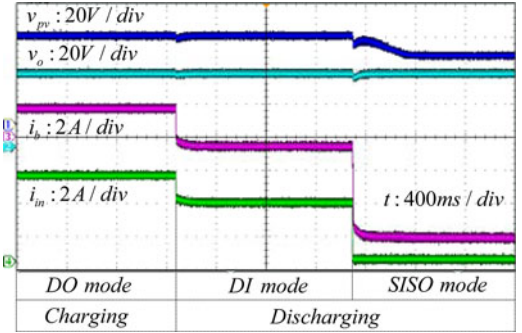


Fig. 15. Waveforms of operation mode transition: Dual-output mode to dual-input mode and then to single-input single-output mode.

switches between DI mode and DO mode, and the battery transients between charging mode and discharging mode. The input power is kept constant, and the output voltage is stable during the load transient as while the battery current/power varies to compensate for the load power. The operation mode switching among the DO, DI, and SISO are also tested, and the waveforms are given in Fig. 15. It can be seen that the output voltage v_o is always tightly controlled under every operation mode and also during mode transients.

The efficiency curves of the converter at full-load condition are given in Fig. 16. Fig. 16(a) is the efficiency with different battery power while $v_{pv} = 60$ V and $v_b = 30$ V. A positive value of the battery power indicates that the battery is in the charging mode, while a negative value indicates that it is in the discharging mode, the efficiency drops dramatically while battery discharging because the battery voltage v_b is much lower than the solar voltage, and when the battery discharges the conduction loss will increase dramatically. Fig. 16(b) is the efficiency over the full input voltage range. It can be seen that when input voltage decreases, the efficiency also drops because of the increase of conduction loss.

V. EXTENSION OF THE PROPOSED TOPOLOGY CONCEPT

A. Variation of the Primary Circuit of the FB-TPC

Fig. 1(c) gives the FB-TPC with the two cells, cells A and B, sharing the negative terminals. Because the two cells as well as the two sources of the FB-TPC are independent, they can also

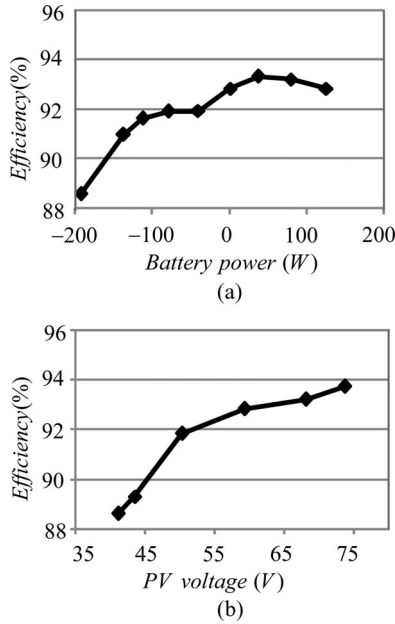


Fig. 16. Efficiency curves, under full-load condition, versus (a) battery power and (b) input voltage.

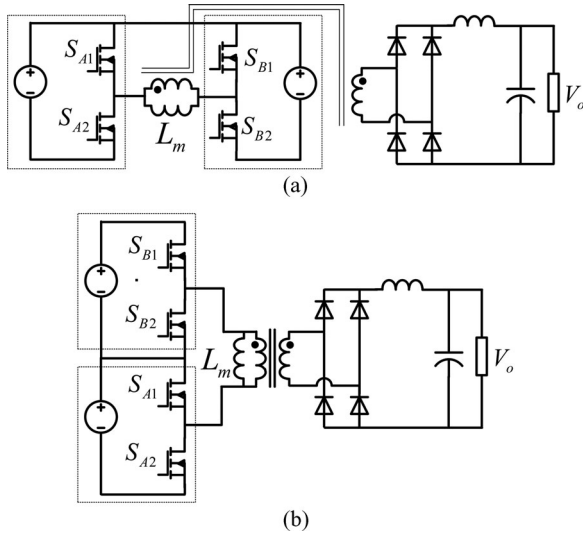


Fig. 17. Two FB-TPCs with the two cells (a) sharing the positive terminals and (b) connected in series.

be connected in other manners. The other two types of FB-TPCs are shown in Fig. 17. The operation principles of these FB-TPCs are similar.

B. Improvement of the FB-TPC

The key characteristic of the FB-TPC is that the magnetizing inductor of the transformer also functions as a filter inductor, and the primary circuit acts as a four-switch buck-boost converter to bridge the power flow between the two ports on the primary side. However, the energy storage ability of the transformer may limit the power rating of the FB-TPC. To overcome this drawback, a block capacitor can be placed in series with the primary winding and another optimally designed inductor placed in parallel with

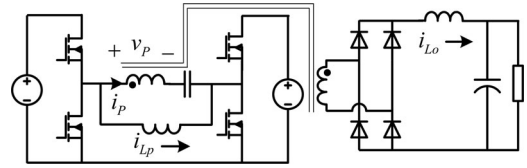


Fig. 18. Topology of the FB-TPC with paralleled inductor (FB-TPC-PI).

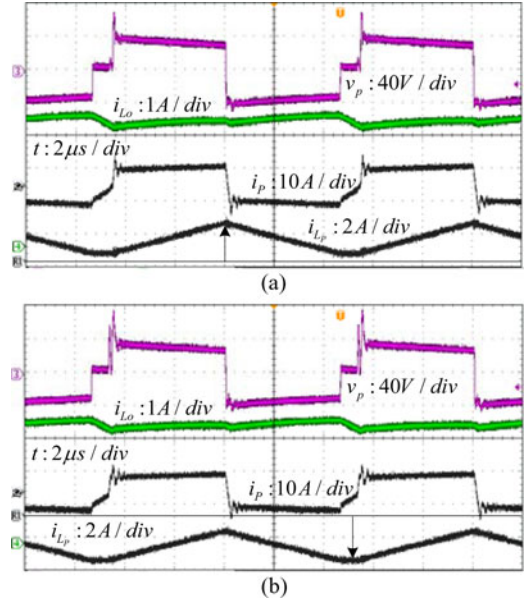


Fig. 19. Steady-state waveforms of the FB-TPC-PI in (a) dual-output mode and (b) dual-input mode.

the transformer to transfer power between the primary side's two ports, as shown in Fig. 18. The improved converter, named FB-TPC with a paralleled inductor (FB-TPC-PI), can be seen as a combination of a four-switch buck-boost converter and an FBC with shared power switches. It is suitable for the higher power application but another inductor is required which may degrade the power density of the converter.

The control and operation principles of the FB-TPC-PI are the same as the FB-TPC. To verify the operation of the FB-TPC-PI, a prototype of the FB-TPC-PI is also built with the same parameters shown in Table II. The values of block capacitor and paralleled inductor of the FB-TPC-PI are 4 μF and 55 μH, respectively. The steady-state waveforms with 70 V input voltage at full load are given in Fig. 19. Fig. 19(a) is the waveforms of the DO mode. Fig. 19(b) shows the waveforms of the DI mode. It can be seen that the difference between these two modes is the dc value of i_{Lp}, which is similar to the waveforms of the FB-TPC, as shown in Fig. 11. The efficiency under the full load with different input voltages is given in Fig. 20. The efficiency of the FB-TPC-PI is higher than that of the FB-TPC because a paralleled inductor is introduced and the conduction loss of the transformer's primary winding can be decreased.

C. DI and Multiport Converters

If the primary side's two ports do not need to transfer the power between each other, the paralleled inductor can be

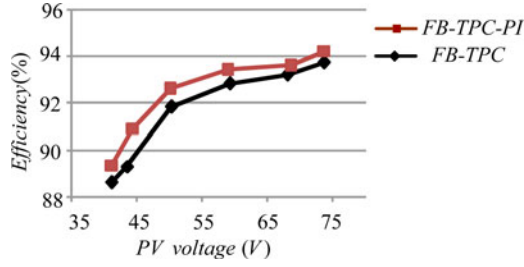


Fig. 20. Efficiency curves, under full power, versus PV source voltage.

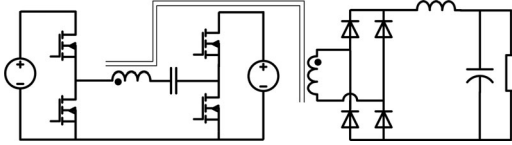


Fig. 21. Proposed dual-input full-bridge converter.

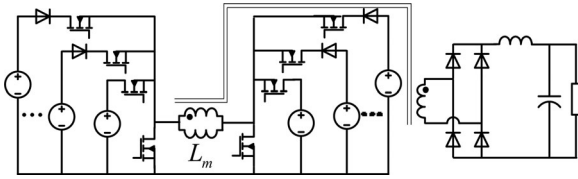


Fig. 22. Multiport full-bridge converter.

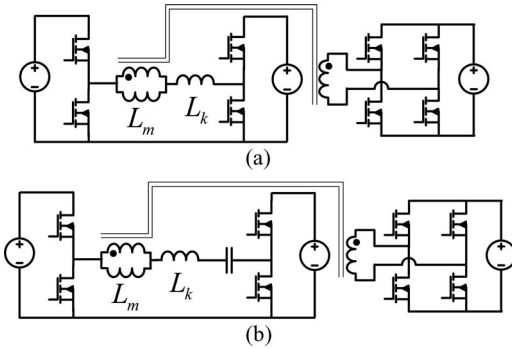


Fig. 23. Converters derived from dual-active-bridge converter. (a) Three-port converter. (b) Dual-input converter.

removed, and then a DI FBC can be derived, as shown in Fig. 21. With this topology, the two sources can supply power to the load alternately or simultaneously. Similar to the multi-input four-switch buck-boost converter [25], the number of input ports of the FB-TPC can also be extended, and the input ports can be added to both of the primary side's two ports, as shown in Fig. 22, because the converter has a symmetrical structure.

The improvement and variation is also valid for the other two FB-TPCs shown in Fig. 17.

D. New Topologies Derived From DAB Converters

The proposed topology concept, splitting the switching legs of the FBC and connecting to different sources to generate the TPC or DI converter, can be applied to other topologies with full-bridge structure, such as the DAB converter [12] and the

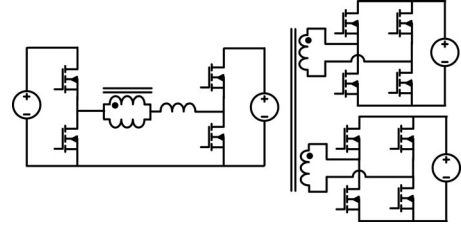


Fig. 24. Four-port full-bridge converter.

three-port FBC [10]. Taking the DAB converter as an example, the derived TPC and DI converter are given in Fig. 23(a) and (b), respectively. It should be noted that all three ports of the TPC, shown in Fig. 20(a), are bidirectional. For the three-port FBC, when one of the active bridge is split and connected to different sources, a four-port FBC will be derived, as illustrated in Fig. 24.

VI. CONCLUSION

Novel FB-TPCs have been proposed and investigated in this paper. The FB-TPCs are rooted in the FBC and generated by splitting the two switching legs of the FBC into two switching cells, connecting the two cells to different sources, and utilizing the magnetizing inductance of the transformer as a filter inductor. A buck-boost converter is integrated in the FB-TPC and used to configure the power flow path between the two ports on the primary side of the converter, which is aimed to handle a wide range of source voltage. ZVS has been achieved for all the primary-side switches by utilizing the energy stored in the leakage inductance of the transformer. This results in high conversion efficiency. The topology generation concept is further extended and some novel TPCs and multiport converters are derived. The proposed converters offer the advantages of simple topologies and control, reduced number of devices, and a single-stage power conversion between any two of the three ports. They are suitable for renewable power systems that are sourced by solar, thermoelectric generator, etc., with voltages varying over a wide range.

The analysis of the operating principles and the experimental results of the FB-TPC are given, with the modulation proposed, to verify the proposed topology derivation method.

REFERENCES

- [1] A. Kwasinski, "Quantitative evaluation of DC microgrids availability: Effects of system architecture and converter topology design choices," *IEEE Trans. Power Electron.*, vol. 26, no. 3, pp. 835–851, Mar. 2011.
- [2] W. Jiang and B. Fahimi, "Multi-port power electric interface for renewable energy sources," in *Proc. IEEE Appl. Power Electron. Conf.*, 2009, pp. 347–352.
- [3] W. Jiang and B. Fahimi, "Multiport power electronic interface—Concept, modeling and design," *IEEE Trans. Power Electron.*, vol. 26, no. 7, pp. 1890–1900, Jul. 2011.
- [4] H. Tao, J. L. Duarte, and M. A. M. Hendrix, "Multiport converters for hybrid power sources," *IEEE Proc. Power Electron. Spec. Conf.*, pp. 3412–3418, 2008.
- [5] H. Tao, A. Kotsopoulos, J. L. Duarte, and M. A. M. Hendrix, "Family of multiport bidirectional dc-dc converters," *Inst. Electr. Eng. Proc. Elect. Power Appl.*, vol. 153, no. 15, pp. 451–458, May 2006.

- [6] Z. Qian, O. Abdel-Rahman, H. Al-Atrash, and I. Batarseh, "Modeling and control of three-port DC/DC converter interface for satellite applications," *IEEE Trans. Power Electron.*, vol. 25, no. 3, pp. 637–649, Mar. 2010.
- [7] Z. Qian, O. Abdel-Rahman, H. Hu, and I. Batarseh, "An integrated three-port inverter for stand-alone PV applications," presented at the *IEEE Energy Convers. Congr. Expo.*, Atlanta, GA, 2010.
- [8] H. Wu, R. Chen, J. Zhang, Y. Xing, H. Hu, and H. Ge, "A family of three-port half-bridge converters for a stand-alone renewable power system," *IEEE Trans. Power Electron.*, vol. 26, no. 9, pp. 2697–2706, Sep. 2011.
- [9] C. Zhao, S. D. Round, and W. Johann, "An isolated three-port bidirectional DC-DC converter with decoupled power flow management," *IEEE Trans. Power Electron.*, vol. 23, no. 5, pp. 2443–2453, Sep. 2008.
- [10] J. L. Duarte, M. A. M. Hendrix, and M. G. Simoes, "Three-port bidirectional converter for hybrid fuel cell systems," *IEEE Trans. Power Electron.*, vol. 22, no. 2, pp. 480–487, Mar. 2007.
- [11] H. Tao, J. L. Duarte, and A. M. Marcel, "Three-port triple-half-bridge bidirectional converter with zero-voltage switching," *IEEE Trans. Power Electron.*, vol. 23, no. 2, pp. 782–792, Mar. 2008.
- [12] H. Tao, A. Kotsopoulos, J. Duarte, and M. Hendrix, "Transformer-coupled multiport ZVS bidirectional dc-dc converter with wide input range," *IEEE Trans. Power Electron.*, vol. 23, no. 2, pp. 771–781, Mar. 2008.
- [13] K. Haribaran and N. Mohan, "Three-port series-resonant DC-DC converter to interface renewable energy sources with bidirectional load and energy storage ports," *IEEE Trans. Power Electron.*, vol. 24, no. 10, pp. 2289–2297, 2009.
- [14] D. Liu and H. Li, "A ZVS bi-directional DC-DC converter for multiple energy storage elements," *IEEE Trans. Power Electron.*, vol. 21, no. 5, pp. 1513–1517, Sep. 2006.
- [15] S. Falcones and R. Ayyanar, "Simple control design for a three-port DC-DC converter based PV system with energy storage," presented at the *IEEE Appl. Power Electron. Conf.*, Palm Springs, CA, 2010.
- [16] F. Z. Peng, H. Li, G. J. Su, and J. Lawler, "A new ZVS bi-directional dc-dc converter for fuel cell and battery application," *IEEE Trans. Power Electron.*, vol. 19, no. 1, pp. 54–65, Jan. 2004.
- [17] D. Xu, C. Zhao, and H. Fan, "A PWM plus phase-shift control bidirectional dc-dc converter," *IEEE Trans. Power Electron.*, vol. 19, no. 5, pp. 666–675, May 2004.
- [18] H. Al-Atrash and I. Batarseh, "Boost-integrated phase-shift full-bridge converter for three-port interface," in *Proc. IEEE Power Electron. Spec. Conf.*, 2007, pp. 2313–2321.
- [19] Z. Wang and H. Li, "Integrated MPPT and bidirectional battery charger for PV application using one multiphase interleaved three-port DC-DC converter," in *Proc. 26th IEEE Appl. Power Electron. Conf. Expo.*, 2011, pp. 295–300.
- [20] S. Waffler and J. W. Kolar, "A novel low-loss modulation strategy for high-power bidirectional Buck+Boost converters," *IEEE Trans. Power Electron.*, vol. 24, no. 6, pp. 1589–1599, Jun. 2009.
- [21] Y. Lee, A. Khaligh, A. Chakraborty, and A. Emadi, "Digital combination of buck and boost converters to control a positive buck-boost converter and improve the output transients," *IEEE Trans. Power Electron.*, vol. 24, no. 5, pp. 1267–1279, May 2009.
- [22] S. Lim and A. Q. Huang, "Design of a transient voltage clamp (TVC) for 4 switch buck boost (4SBB) converter," in *Proc. IEEE Energy Convers. Congr. Expo.*, 2009, pp. 659–661.
- [23] E. Kim and Y. Kim, "A ZVZCS PWM FB DC/DC converter using a modified energy-recovery snubber," *IEEE Trans. Ind. Electron.*, vol. 49, no. 5, pp. 1120–1127, Oct. 2002.
- [24] B.-Y. Chen and Y. S. Lai, "Switching control technique of phase-shift-controlled full-bridge converter to improve efficiency under light-load and standby conditions without additional auxiliary components," *IEEE Trans. Power Electron.*, vol. 25, no. 4, pp. 1001–1012, Apr. 2010.
- [25] A. Khaligh, J. Cao, and Y. Lee, "A multiple input DC-DC converter topology," *IEEE Trans. Power Electron.*, vol. 24, no. 3, pp. 862–868, Mar. 2009.



Hongfei Wu (S'11) was born in Hebei, China, in 1985. He received the B.S. degree in electrical engineering from the Nanjing University of Aeronautics and Astronautics, Nanjing, China, in 2008, where he is currently working toward the Ph.D. degree in electrical engineering.

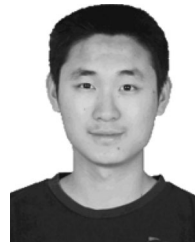
His research interests include topology and control of dc-dc converters and soft-switching dc-dc converters.



tor drives.

Kai Sun (M'12) received the B.E., M.E., and Ph.D. degrees in electrical engineering from Tsinghua University, Beijing, China, in 2000, 2002, and 2006, respectively.

In 2006, he became a Lecturer on Electrical Engineering with the faculty of Tsinghua University. From September 2009 to August 2010, he was a Visiting Scholar of Electrical Engineering at the Institute of Energy Technology, Aalborg University, Aalborg, Denmark. His research interests include power converters, distributed generation technology, and ac motor drives.



Runruo Chen was born in Jiangsu, China, in 1989. He received the B.S. degree in electrical engineering from the Nanjing University of Aeronautics and Astronautics, Nanjing, China, in 2011, where he is currently working toward the M.S. degree in electrical engineering.

His main research interests include topology and control of dc-dc converters.



Haibing Hu (M'09) received the B.S. degree from the Hunan University of Technology, Hunan, China, in 1995, and the M.S. and Ph.D. degrees in electrical engineering from Zhejiang University, in 2003 and 2007, respectively.

From 2007 to 2009, he was an Assistant Professor in the Department of Control Engineering, Nanjing University of Aeronautics and Astronautics, Nanjing, China, where he is currently an Associate Professor. In 2009, he was a Senior Research Fellow in the Department of Electrical Engineering, University of

Central Florida. He is the author or coauthor of more than 40 technical papers published in journals and conference proceedings. His research interests include digital control in power electronics, multilevel inverter, digital control system integration for power electronics, and applying power electronics to distributed energy systems and power quality.



Yan Xing (M'03) was born in Shandong, China, in 1964. She received the B.S. and M.S. degrees in automation and electrical engineering from Tsinghua University, Beijing, China, in 1985 and 1988, respectively, and the Ph.D. degree in electrical engineering from the Nanjing University of Aeronautics and Astronautics (NUAA), Nanjing, China, in 2000.

Since 1988, she has been with the Faculty of Electrical Engineering, NUAA, where she is currently a Professor at the Aero-Power Sci-Tech Center, College of Automation Engineering. She is the author of

more than 60 technical papers published in journals and conference proceedings and has also published three books. Her research interests include topology and control for dc-dc and dc-ac converters.